Topological Exact Flat Bands in Two-Dimensional Materials under Periodic Strain

Xiaohan Wan, Siddhartha Sarkar, Shi-Zeng Lin, and Kai Sun

Topological exact flat bands in two dimensional materials under periodic strain

Xiaohan Wan,[1, 2] Siddhartha Sarkar,[1] Shi-Zeng Lin,[2, 3, *] and Kai Sun[1, †]

[1]*Department of Physics, University of Michigan, Ann Arbor, MI 48109, USA*
[2]*Theoretical Division, T-4 and CNLS, Los Alamos National Laboratory, Los Alamos, New Mexico 87545, USA*
[3]*Center for Integrated Nanotechnologies (CINT),*
Los Alamos National Laboratory, Los Alamos, New Mexico 87545, USA

We study flat bands and their topology in 2D materials with quadratic band crossing points (QBCPs) under periodic strain. In contrast to Dirac points in graphene, where strain acts as a vector potential, strain for QBCPs serves as a director potential with angular momentum $\ell = 2$. We prove that when the strengths of the strain fields hit certain "magic" values, exact flat bands with $C = \pm 1$ emerge at charge neutrality point in the chiral limit, in strong analogy to magic angle twisted bilayer graphene. These flat bands have ideal quantum geometry for the realization of fractional Chern insulators, and they are always fragile topological. The number of flat bands can be doubled for certain point group, and the interacting Hamiltonian is exactly solvable at integer fillings. We further demonstrate the stability of these flat bands against deviations from the chiral limit, and discuss possible realization in 2D materials.

Introduction.– Electronic band structures of 2D materials can be controlled and designed by manipulating superlattice structures. One well-known example is twisted bilayer graphene (TBG), where interference between the two layers makes the band structure angle dependent. Remarkably, at some "magic angles", isolated nearly flat topological bands arise [1–3], which become exactly flat in the chiral limit [4], and similar flat bands may arise in other twisted-bilayer systems as well, such as quadratic band crossing point (QBCP) bilayers [5, 6]. This property of twisted bilayers makes them an exciting platform for studying strongly correlated phenomena such as unconventional superconductivity and correlated insulators [7–31]. In single layer moiré systems, exciting progress towards similar interference has been achieved via spatially varying electrostatic field, magnetic field, and elastic strain field [32–43]. However, for these systems, it was recently argued [41] that (without a constant background magnetic field) exact flat bands cannot be achieved even in the chiral limit.

In this Letter, we study single layer systems with QBCPs under periodic strains. In contrast to Dirac points in graphene, where strain serves as a vector potential via minimal coupling $i\partial \to i\partial + A$ [44], for QBCPs at time-reversal invariant momenta, such gauge-field-like couplings are prohibited by the time-reversal symmetry. Because $i\partial$ and strain fields have opposite parity under time reversal, the couplings allowed by symmetry for QBCPs take the form of $\partial\partial \to \partial\partial + A$, where A is proportional to the strain field. In other words, the strain fields here provide a director potential with angular momentum $\ell = 2$, instead of a vector with $\ell = 1$.

Remarkably, we find that this strain-field coupling induces exact flat bands, in strong analogy to TBG. Here, instead of controlling the twisting angle, we vary the strength of the strain field. In the chiral limit, exact flat bands are obtained as the strength of the strain field hits certain "magic" values, and the flat bands carry Chern

numbers $C = \pm 1$. Away from the chiral limit, these magic flat bands survive in a wide range of phase space, although their bandwidth is no longer exactly zero. We prove analytically that these exact flat bands are protected by the same mathematical principles as magic flat bands in TBG, and thus in analogy to TBG, they are fragile topological bands and their quantum metric satisfy the trace condition. In addition, we find that their Berry curvature distributions are more uniform than the TBG flat bands, making them ideal for the realization of fractional Chern insulators [45–51].

Despite these similarities, it is also worth highlighting that these strain-induced flat bands are due to a very different physical mechanism, and thus they exhibit some unique physical properties, sharply distinct from TBG. For example, these strain-induced flat bands can arise at the Γ valley and only need a single layer, while twisted-bilayer magic flat bands require a finite wave vector away from Γ [52] and interference between two layers. Secondly, twisted bilayer magic flat bands arise for various dispersion, e.g., Dirac and QBCP [5], while the strain-induced magic flat bands can only emerge from QBCPs.

QBCP, strain field and director potential.– Without requiring fine tuning, a stable QBCP can only arise at time-reversal (T) invariant momenta ($T\mathbf{k} = -\mathbf{k}$) with proper rotational symmetry [53], where T and rotational symmetries protect the QBCP from being gapped out or splitting into Dirac points [53–55]. Here we will focus on a QBCP with T and 3- or 6-fold rotational symmetry, e.g., the Γ point of a kagome metal. Up to a change of basis, the Hamiltonian near Γ takes the following form

$$H_\Gamma = -t_0 a^2 \left(c_0 k^2 \mathbb{1} - (k_x^2 - k_y^2)\sigma_x - 2k_x k_y \sigma_y \right), \quad (1)$$

where $\mathbb{1}$, σ_x, σ_y represent the 2×2 identity and Pauli matrices respectively, and $k = |\mathbf{k}|$. Without loss of generality, we set $t_0 = 1$ and $a = 1$. Here, c_0 determines the average effective mass of the two bands. At $c_0 = 0$, a chiral symmetry emerges, $\{H, \sigma_z\} = 0$, and thus the
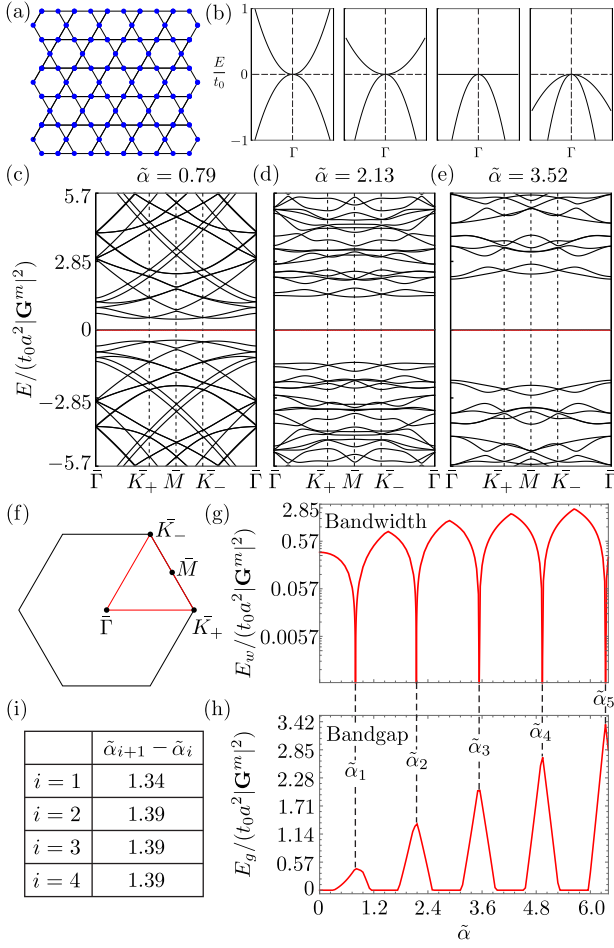
FIG. 1. Exact flat bands from a QBCP under periodic strain. (a) Schematic of a kagome lattice, which has a QBCP at Γ. (b) The band structure of a QBCP [Eq. (1)] at $c_0 = 0, 0.5, 1, 1.5$, where $c_0 = 0$ is the chiral limit. (c-e) Band structures in the chiral limit under strain $\tilde{A}$ [Eq. 3 at $\phi = 0$] at different critical values of $\tilde{\alpha} = \alpha/(|\mathbf{G}^m|a)$ along the high symmetry path in the Moiré Brillouin zone shown in (f). There are two exact flat bands at $E = 0$ in each case. (g,h) Bandwidth E_w and bandgap E_g as a function of $\tilde{\alpha}$, respectively. The bandwidth is exactly zero at the critical values of $\tilde{\alpha}$. The minima of the bandwidth occur at the same values of $\tilde{\alpha}$ as the maxima of the bandgap. (i) Table of the values of $\Delta\tilde{\alpha} = \tilde{\alpha}_{i+1} - \tilde{\alpha}_i$.

dispersion of the two bands is symmetric around $E = 0$. A nonzero c_0 breaks the chiral symmetry with dispersion similar to a kagome metal (Fig. 1(b)). The special case of $c_0 = \pm 1$ generates a flat band, as in the nearest-neighbor-hopping kagome lattice [Fig. 1(a), also Supplemental material (SM) [56]].

Under a slowly varying strain field $u_{ij}(\mathbf{r})$, the Hamiltonian becomes

$$H(\mathbf{r}) = H_\Gamma + A_I(\mathbf{r})\mathbb{1} + A_x(\mathbf{r})\sigma_x + A_y(\mathbf{r})\sigma_y,$$
$$= \begin{pmatrix} 4c_0\partial_z\partial_{\bar{z}} + A_I & 4\partial_z^2 + \tilde{A} \\ 4\partial_{\bar{z}}^2 + \tilde{A}^* & 4c_0\partial_z\partial_{\bar{z}} + A_I \end{pmatrix}, \qquad (2)$$

where $A_I \propto u_{xx} + u_{yy}$ describes bulk deformation, and $A_x \propto u_{xx} - u_{yy}$ and $A_y \propto u_{xy}$ describe shear deformations. Here we introduce complex coordinates and strains $z = x + iy$ and $\tilde{A} = A_x - iA_y$. Here, $\tilde{A}$ couples to $(k_x - ik_y)^2$, which is a director with angular momentum $\ell = 2$. This director potential is the key reason why periodic strain can induce magic flat bands for QBCPs. In SM [56], we demonstrate a specific example using a kagome lattice tight-binding model to explicitly derive this Hamiltonian and the director potential coupling.

C_{3v} symmetric and the chiral limit.– We start from the chiral limit $c_0 = A_I = 0$ and show that periodic strains lead to exact flat bands. A real physical system in general deviates from this ideal limit, but as is shown below, as long as such deviation is not too severe, magic flat bands still remain. Before studying this chiral limit, it is worth commenting on how to achieve this limit. To make c_0 close to zero, we need to use materials where the two bands near a QBCP have opposite effective mass (e.g., $GaCu_3(OH)_6Cl_2$ [57]). To make $A_I << A_x$ or A_y, it simply requires to use 2D materials with a bulk modulus (B) larger than the shear modulus (G), so that shear deformations (A_x and A_y) have lower energy cost than bulk deformation (A_I). In typical materials, this condition $B > G$ is naturally satisfied, unless the material is auxetic, i.e., has negative Poisson ratio.

In the chiral limit, we apply a periodic strain with C_{3v} symmetry. Such strain fields can be categorized into two classes depending on whether the mirror plane is parallel or perpendicular to the reciprocal lattice vector $\mathbf{G}^m$. The first category (parallel) includes space groups $p3m1$ and $p6mm$, while the latter (perpendicular) gives $p31m$. Here we will focus on the first category. Within the first harmonic approximation, the strain can be written as

$$\tilde{A}(\mathbf{r}) = t_0 \frac{\alpha^2}{2} \sum_{n=1}^{3} \omega^{n-1} \, \cos\left(\mathbf{G}_n^m \cdot \mathbf{r} + \phi\right), \qquad (3)$$

where $\alpha^2 > 0$ is the strength of the strain, ϕ is an arbitrary phase and $\omega = \exp(2\pi i/3)$. $\mathbf{G}_1^m = \frac{4\pi}{\sqrt{3}a^m}(0,1)$, $\mathbf{G}_{2,3}^m = \frac{4\pi}{\sqrt{3}a^m}(\mp\sqrt{3}/2, -1/2)$ are the reciprocal lattice vectors. The second category has similar exact flat bands (see SM [56]) and its strain field is

$$\tilde{A}(\mathbf{r}) = \pm t_0\alpha^2 \sum_{n=1}^{3} \omega^{n-1} \, \exp\left(i\mathbf{G}_n^m \cdot \mathbf{r}\right). \qquad (4)$$

Exact flat bands at $\phi = 0$.–We start by considering a special case with $\phi = 0$ in Eq. (3), where the system exhibits a higher rotational symmetry C_{6v}. As shown in Fig. 1(c-e), two exactly flat bands with $E = 0$ arise at critical values of α (the square root of the strain strength). We define a dimensionless parameter $\tilde{\alpha} = \alpha/(|\mathbf{G}^m|a)$, which fully controls the physics of the system. These critical $\tilde{\alpha}$'s are roughly equally spaced $\Delta\tilde{\alpha} \approx 1.39$ [Fig. 1(g, i)], and they also maximize the band gap that separates these two
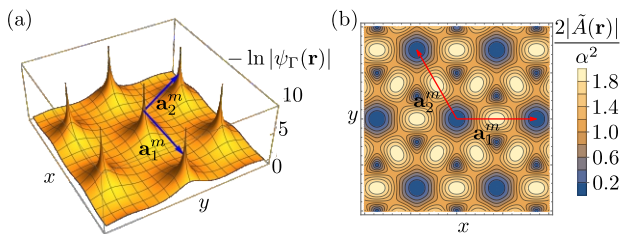
FIG. 2. (a) The plot of $\ln(1/|\psi_\Gamma(\mathbf{r})|)$ at the critical value $\tilde{\alpha} \approx 0.79$ for $\tilde{A}$ in Eq. (3) with $\phi = 0$. The spikes imply that $\psi_\Gamma(\mathbf{r})$ has zeros at $\mathbf{r} = n_1\mathbf{a}_1^m + n_2\mathbf{a}_2^m$, $n_1, n_2 \in \mathbb{Z}$. Here, $\mathbf{a}_1^m$ and $\mathbf{a}_2^m$ are the lattice vectors of superlattice. (b) Contour plot of $\frac{2|\tilde{A}(\mathbf{r})|}{\alpha^2}$.

flat bands from others [Fig. 1(h)]. In analogy to TBG in the chiral limit [4, 41], these critical strains and exact flat bands can be analytically proved, and their Bloch wavefunctions can be analytically constructed. We start from the Γ point. Because the strain preserves T and C_3 symmetry, the two-fold degeneracy of the QBCP remains. In the chiral limit, the energy of these two degenerate states must remain at $E = 0$, and their wavefunctions can be obtained from the Hamiltonian Eq. (2): $\Psi_{\Gamma,1}(\mathbf{r}) = \{\psi_\Gamma(\mathbf{r}), 0\}$ and $\Psi_{\Gamma,2}(\mathbf{r}) = \{0, \psi_\Gamma^*(\mathbf{r})\}$, where $\psi_\Gamma(\mathbf{r})$ is a periodic function of the superlattice and obeys $(4\partial_{\bar{z}}^2 + \tilde{A}^*)\psi_\Gamma(\mathbf{r}) = 0$. $\Psi_{\Gamma,1}$ and $\Psi_{\Gamma,2}$ are related with each other via time-reversal, $T = \sigma_x K$, where K is the complex conjugation.

If there are exact flat bands at $E = 0$, the eigenfunctions can be written as $\{\psi_\mathbf{k}(\mathbf{r}), 0\}$ and $\{0, \psi_{-\mathbf{k}}^*(\mathbf{r})\}$ with $(4\partial_{\bar{z}}^2 + \tilde{A}^*)\psi_\mathbf{k}(\mathbf{r}) = 0$. Since the kinetic part of $D^\dagger(\mathbf{r})$ is antiholomorphic, we can construct a trial wave-function $\psi_\mathbf{k}(\mathbf{r}) = f_\mathbf{k}(z)\psi_\Gamma(\mathbf{r})$. The $f_\mathbf{k}(z)$ needs to satisfy Bloch periodicity (translation by a superlattice vector $\mathbf{a}^m$ gives a phase shift of $e^{i\mathbf{k}\cdot\mathbf{a}^m}$). However, from Liouville's theorem, such $f_\mathbf{k}(z)$ must have poles, making $\psi_\mathbf{k}(\mathbf{r})$ divergent. To avoid such singularity, $\psi_\Gamma(\mathbf{r})$ needs to have a zero that cancels the pole of $f_\mathbf{k}(z)$. As shown in Fig. 2(a), at the magic values of $\tilde{\alpha}_i$, $\psi_\Gamma(\mathbf{0}) = 0$. Hence, we have

$$\Psi_{\mathbf{k},1}(\mathbf{r}) = \begin{bmatrix} \psi_\mathbf{k}(\mathbf{r}) \\ 0 \end{bmatrix}, \Psi_{\mathbf{k},2}(\mathbf{r}) = \begin{bmatrix} 0 \\ \psi_{-\mathbf{k}}^*(\mathbf{r}) \end{bmatrix},$$
$$\psi_\mathbf{k}(\mathbf{r}) = \frac{\vartheta_{\frac{\mathbf{k}\cdot\mathbf{a}_1^m}{2\pi}-\frac{1}{2}, \frac{1}{2}-\frac{\mathbf{k}\cdot\mathbf{a}_2^m}{2\pi}}\left(\frac{z}{a_1}, \omega\right)}{\vartheta_{-\frac{1}{2}, \frac{1}{2}}\left(\frac{z}{a_1}, \omega\right)} \psi_\Gamma(\mathbf{r}), \quad (5)$$

where $\vartheta_{a,b}(z, \tau)$ is the theta function of rational characteristic [58], $\mathbf{a}_i^m$ are lattice vectors ($\mathbf{a}_1^m = a^m(1, 0)$, $\mathbf{a}_2^m = a^m(-1, \sqrt{3})/2$) of the superlattice, $a_i = (\mathbf{a}_i^m)_x + i(\mathbf{a}_i^m)_y$. As shown in the SM [56], these wavefunctions give two exact flat bands with $E = 0$.

In analogy to the Chern basis in TBGs [59], because these two flat bands only involve holomorphic or antiholomorphic functions, they have Chern number ± 1. Same as Landau levels, their Fubini-Study metric $g(\mathbf{k})$ satisfies the trace condition $\text{tr}(g(\mathbf{k})) = |F_{xy}(\mathbf{k})|$ [46–51], where

$F_{xy}(\mathbf{k})$ is the Berry curvature (see SM. Sec. III [56]). In SM Fig. S1 [56], the distributions of the Berry curvature in k-space are shown for the first three critical $\tilde{\alpha}$, which we found to be quite uniform. To quantify the non-uniformity of Berry curvature, we measure the ratio between the root-mean-square deviation of the Berry curvature and its average value $\Delta F_{xy}/\bar{F}_{xy}$ [45]. The smallest value (most uniform distribution) is found at the second critical $\tilde{\alpha}$ with $\Delta F_{xy}/\bar{F}_{xy} \approx 0.027$, much smaller than the reported values in TBG flatbands [47]. Ideal quantum metric and very uniform Berry curvature make this system an ideal candidate for realizing fractional Chern insulators [45–51].

Generic ϕ, double zeros and 4-fold flat bands.- In addition to $\phi = 0$ (Eq. (3), exact flat bands also arise at $\phi \neq 0$. At $\phi = n\pi/3$ ($\phi \neq n\pi/3$), the strain preserves 6-fold (3-fold) rotational symmetry with space group symmetry $p6mm$ ($p3m1$). In Fig. 3(a), we plot the bandwidth as a function of $\tilde{\alpha}^2$ and ϕ in polar coordinate, setting $\tilde{\alpha}^2$ and ϕ to be the radius and polar angle, respectively. The dark lines mark the exact flat bands and the dashed green line marks analytic solution from perturbation theory (See SM [56]). As we can see, for any value of ϕ, exact flat bands can be reached at certain critical field strengths.

To further verify this conclusion, we show that $\psi_\Gamma(\mathbf{r})$ indeed contains zeros for all critical $\tilde{\alpha}$'s, and thus analytic wavefunctions can be constructed for these exact flat bands following the same procedure shown above. In Figs. 3(c-e), we plot in log scale $|\psi_\Gamma(\mathbf{r} = \mathbf{0})|$, $|\psi_\Gamma(\mathbf{r} = (2\mathbf{a}_1^m + \mathbf{a}_2^m)/3)|$ and $|\psi_\Gamma(\mathbf{r} = (2\mathbf{a}_2^m + \mathbf{a}_1^m)/3)|$, as well as $\min\{|\psi_\Gamma(\mathbf{r} = \mathbf{0})|, |\psi_\Gamma(\mathbf{r} = (2\mathbf{a}_2^m + \mathbf{a}_1^m)/3)|, |\psi_\Gamma(\mathbf{r} = (2\mathbf{a}_1^m + \mathbf{a}_2^m)/3)|\}$ in Fig. 3(b). These three real space points are the 3-fold rotation centers of the $p3m1$ lattice, and the dark lines in these figures mark $\psi_\Gamma = 0$, which perfectly match the exact flat bands shown in Fig. 3(a).

The reason, we only see $\psi_\Gamma = 0$ at these three high symmetry points in the unit cell, is that ψ_Γ at other $\mathbf{r}$ are in general complex. To make both the real and imaginary parts zero, it typically requires to adjust two real control parameters simultaneously. In contrast, ψ_Γ at these high symmetry points must be real, due to the T and C_{3v} symmetry (See SM [56]), and thus its value can be tuned to zero with only one control parameter, which is why exact flat bands can emerge as we scan $\tilde{\alpha}$. This is why the addition of mirror symmetry to C_3 and T is important.

It is easy to check that for these periodic strain fields, there exists a symmetry of $\phi \rightarrow \phi + 2\pi/3$. This transformation corresponds to a real space translation that swaps the three real-space high-symmetry points $\mathbf{0}$, $(2\mathbf{a}_1^m + \mathbf{a}_2^m)/3$, and $(2\mathbf{a}_2^m + \mathbf{a}_1^m)/3$, as can be seen from Figs. 3(c-e). This is the reason why Figs. 3(a) and (b) are three-fold symmetric. At points highlighted by the red circles in Fig. 3(b), $\psi_\Gamma(\mathbf{r})$ has 2 zeros in a unit cell (two of the three real-space high-symmetry points). These double zeros are not accidental but due
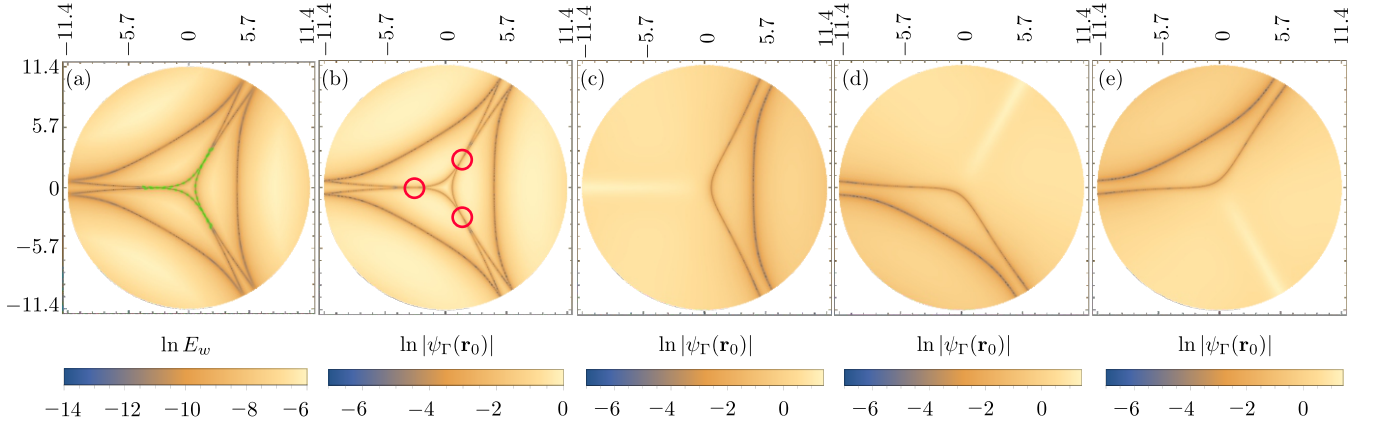
FIG. 3. Exact flat bands in polar coordinate of $\tilde{\alpha}^2$ (radius) and ϕ (polar angle). (a) Bandwidth $\ln E_w$ as a function of ϕ and $\tilde{\alpha}$. The green dashed line shows the predicted value of principal critical $\tilde{\alpha}$ from 9th order perturbation theory. (b) $\min\{\ln|\psi_\Gamma(\mathbf{r}=\mathbf{0})|, \ln|\psi_\Gamma(\mathbf{r}=(2\mathbf{a}_2^m+\mathbf{a}_1^m)/3)|, \ln|\psi_\Gamma(\mathbf{r}=(2\mathbf{a}_1^m+\mathbf{a}_2^m)/3)|\}$ as a function of $\tilde{\alpha}$ and ϕ. (c-e) $\ln|\psi_\Gamma(\mathbf{r}=\mathbf{0})|$, $\ln|\psi_\Gamma(\mathbf{r}=(2\mathbf{a}_1^m+\mathbf{a}_2^m)/3)|$, $\ln|\psi_\Gamma(\mathbf{r}=(2\mathbf{a}_2^m+\mathbf{a}_1^m)/3)|$ as a function of $\tilde{\alpha}$ and ϕ. The dark lines in each plot show critical $\tilde{\alpha}$ with two exact flat bands. At the crossing point of two dark lines [red circles in (b)], the strain induces four degenerate flat bands.

to the rotational symmetry. For example, at $\phi = \pi$, the rotational symmetry of the system increases to 6-fold and two of the high symmetry points, $(2\mathbf{a}_2^m+\mathbf{a}_1^m)/3$ and $(2\mathbf{a}_1^m+\mathbf{a}_2^m)/3$, are connected by this 6-fold rotation. Thus, when $\psi_\Gamma(\mathbf{r}=(2\mathbf{a}_2^m+\mathbf{a}_1^m)/3)$ reaches zero at $\tilde{\alpha} \approx 1.695$, so does $\psi_\Gamma(\mathbf{r}=(2\mathbf{a}_1^m+\mathbf{a}_2^m)/3)$ (see SM. Fig. S3(d) [56] for the plot of $\psi_\Gamma(\mathbf{r})$). With two zeros, we can construct two meromorphic Bloch-periodic functions $f_{\mathbf{k}}^{(1)}(z)$ and $f_{\mathbf{k}}^{(2)}(z)$ similar to Eq. (5). Hence there are four flat bands instead of two, as is shown in SM. Fig. S3 [56]. For completeness, we also plotted the predicted values of smallest critical $\tilde{\alpha}$ from 9th order perturbation theory in Fig. 3(a) (green dashed lines, see SM. Sec. VII [56] for details), they agree very well with the numerically calculated critical $\tilde{\alpha}$.

Fragile topology and exact solutions in interacting systems– As shown in SM Sec. IX-X [56], in analogy to flat bands in TBG [2, 3, 59], these flat bands are fragile topological bands. In addition, For spin-1/2 fermions with charge repulsion, these flat bands exhibit an emergent U(2)×U(2) symmetry and integer fillings can be solved exactly (see SM Sec. XII [56]), similar to TBG [60–62]. At charge neutrality ($\nu = 0$), there are degenerate ground states with Chern number 0 or ± 2, but thermal fluctuations stabilize the $C = 0$ state via order-by-disorder. At filling $\nu = \pm 1$, the exact ground state is a Chern insulator with $C = \pm 1$.

Breaking chiral symmetry.– In analogy to TBG, as we move away from the chiral limit, these magic flat bands survive, although a small bandwidth emerges. Here we turn on the chiral symmetry breaking term c_0 and A_I in Eq. (2), setting $\tilde{A}$ as Eq. (3) with $\phi = 0$ and $A_I(\mathbf{r}) = -\frac{\alpha^2 c_0 t_0}{4}\sum_{i=1}^3 \cos(\mathbf{G}_i^m \cdot \mathbf{r})$. For a kagome lattice, this A_I naturally arises from nearest-neighbor hoppings (See SM [56]). As shown in Fig. 4, magic flat bands sur-

vive even if c_0 reaches 0.5, although the bandwidth is no longer exactly zero, and the maximum bandgap and the minimum bandwidth slightly misalign. At $\tilde{\alpha} = 0.79$, the bandgap to bandwidth ratio is > 17 for $c_0 = 0.1$ and > 5 for $c_0 = 0.3$. Upon further increasing c_0, these two bands eventually mix with other bands. However, band hybridization and inversion result in an isolated highly flat band at $c_0 = 0.9$ and $\tilde{\alpha} = 1.29$ as shown in SM.
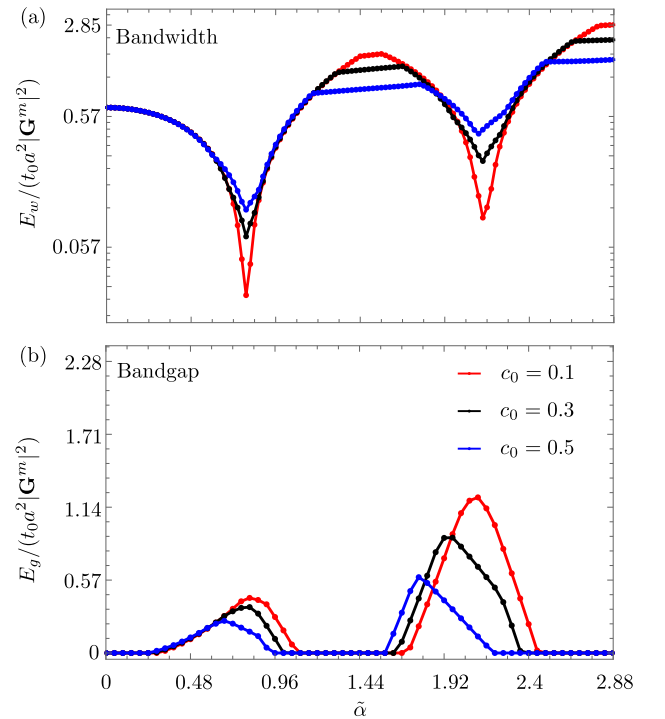

FIG. 4. Effect of chiral symmetry breaking.(a)-(b)Bandwidth E_w and bandgap E_g as a function of $\tilde{\alpha}$ for different c_0.

Fig. S4 [56]. Similarly, for $\tilde{A}$ with $\phi = \pi$ [Eq. (3)] and the same A_I, at $c_0 \approx 0.15$ and $\tilde{\alpha} \approx 1.695$, the four degenerate flat bands around charge neutrality split into two pairs of isolated nearly flat bands as shown in SM. Sec. IX [56], and both of them remain fragile topological, protected by C_2 and C_3, respectively.

Discussions.–In this letter, we studied a QBCP near the Γ point under periodic strain with C_{3v} symmetry, and found exact topological flat bands in the chiral limit. Utilizing materials with nearly-chiral QBCPs (e.g., $GaCu_3(OH)_6Cl_2$ [57]) and a periodic strain field, which has already been achieved in experiments [32, 34], it is possible to access the vicinity of this chiral limit and explore these flat bands, offering a new platform to study topological flat bands, fragile topology, and correlated phases such as fractional Chern insulators and unconventional superconductivity. To further verify the feasibility of this proposal, in SM. Sec. XIV [56], we compared our model with existing experiments and the estimation indicates current strain-engineering technology would allow us to reach at least the first two magic flat bands at the temperature $T \sim 4$ K. In addition, the same principle also applies to other systems with quadratic band crossings, such as photonic/phononic crystals, magnons, and optical lattices [63–67].

Note added: after the submission of this Letter, Ref. [68] showed that similar magic flat bands can arise in QBCP models with 4-fold rotational symmetry.

X.W. and S.S. contributed equally to this work.

―――――――――

* szl@lanl.gov

† sunkai@umich.edu

[1] R. Bistritzer and A. H. MacDonald, Proceedings of the National Academy of Sciences **108**, 12233 (2011).

[2] H. C. Po, H. Watanabe, and A. Vishwanath, Physical review letters **121**, 126402 (2018).

[3] Z. Song, Z. Wang, W. Shi, G. Li, C. Fang, and B. A. Bernevig, Physical review letters **123**, 036401 (2019).

[4] G. Tarnopolsky, A. J. Kruchkov, and A. Vishwanath, Physical review letters **122**, 106405 (2019).

[5] M.-R. Li, A.-L. He, and H. Yao, arXiv preprint arXiv:2111.12107 (2021).

[6] H. Wang, Y. Jiang, Z. Liu, and J. Wang, (2022), arXiv:2209.06524 [cond-mat.mes-hall].

[7] Y. Cao, V. Fatemi, A. Demir, S. Fang, S. L. Tomarken, J. Y. Luo, J. D. Sanchez-Yamagishi, K. Watanabe, T. Taniguchi, E. Kaxiras, *et al.*, Nature **556**, 80 (2018).

[8] Y. Cao, V. Fatemi, S. Fang, K. Watanabe, T. Taniguchi, E. Kaxiras, and P. Jarillo-Herrero, Nature **556**, 43 (2018).

[9] B. Padhi, C. Setty, and P. W. Phillips, Nano letters **18**, 6175 (2018).

[10] X. Lu, P. Stepanov, W. Yang, M. Xie, M. A. Aamir, I. Das, C. Urgell, K. Watanabe, T. Taniguchi, G. Zhang, *et al.*, Nature **574**, 653 (2019).

[11] M. Yankowitz, S. Chen, H. Polshyn, Y. Zhang, K. Watanabe, T. Taniguchi, D. Graf, A. F. Young, and C. R. Dean, Science **363**, 1059 (2019).

[12] H. Polshyn, M. Yankowitz, S. Chen, Y. Zhang, K. Watanabe, C. R. Dean, and A. F. Young, Nature Physics **15**, 1011 (2019).

[13] Y. Xie, B. Lian, B. Jäck, X. Liu, C.-L. Chiu, K. Watanabe, T. Taniguchi, B. A. Bernevig, and A. Yazdani, Nature **572**, 101 (2019).

[14] A. Kerelsky, L. J. McGilly, D. M. Kennes, L. Xian, M. Yankowitz, S. Chen, K. Watanabe, T. Taniguchi, J. Hone, C. Dean, *et al.*, Nature **572**, 95 (2019).

[15] Y. Jiang, X. Lai, K. Watanabe, T. Taniguchi, K. Haule, J. Mao, and E. Y. Andrei, Nature **573**, 91 (2019).

[16] Y. Choi, J. Kemmer, Y. Peng, A. Thomson, H. Arora, R. Polski, Y. Zhang, H. Ren, J. Alicea, G. Refael, *et al.*, Nature Physics **15**, 1174 (2019).

[17] B. Padhi and P. W. Phillips, Physical Review B **99**, 205141 (2019).

[18] Y. Cao, D. Chowdhury, D. Rodan-Legrain, O. Rubies-Bigorda, K. Watanabe, T. Taniguchi, T. Senthil, and P. Jarillo-Herrero, Physical review letters **124**, 076801 (2020).

[19] U. Zondiner, A. Rozen, D. Rodan-Legrain, Y. Cao, R. Queiroz, T. Taniguchi, K. Watanabe, Y. Oreg, F. von Oppen, A. Stern, *et al.*, Nature **582**, 203 (2020).

[20] D. Wong, K. P. Nuckolls, M. Oh, B. Lian, Y. Xie, S. Jeon, K. Watanabe, T. Taniguchi, B. A. Bernevig, and A. Yazdani, Nature **582**, 198 (2020).

[21] K. P. Nuckolls, M. Oh, D. Wong, B. Lian, K. Watanabe, T. Taniguchi, B. A. Bernevig, and A. Yazdani, Nature **588**, 610 (2020).

[22] X. Liu, Z. Hao, E. Khalaf, J. Y. Lee, Y. Ronen, H. Yoo, D. Haei Najafabadi, K. Watanabe, T. Taniguchi, A. Vishwanath, *et al.*, Nature **583**, 221 (2020).

[23] E. C. Regan, D. Wang, C. Jin, M. I. Bakti Utama, B. Gao, X. Wei, S. Zhao, W. Zhao, Z. Zhang, K. Yumigeta, *et al.*, Nature **579**, 359 (2020).

[24] L. Wang, E.-M. Shih, A. Ghiotto, L. Xian, D. A. Rhodes, C. Tan, M. Claassen, D. M. Kennes, Y. Bai, B. Kim, *et al.*, Nature materials **19**, 861 (2020).

[25] M. Xie and A. H. MacDonald, Physical review letters **124**, 097601 (2020).

[26] F. Wu and S. DasSarma, Physical review letters **124**, 046403 (2020).

[27] Y. Su and S.-Z. Lin, Physical Review Letters **125**, 226401 (2020).

[28] N. Stefanidis and I. Sodemann, Physical Review B **102**, 035158 (2020).

[29] N. Bultinck, S. Chatterjee, and M. P. Zaletel, Physical review letters **124**, 166601 (2020).

[30] B. Padhi, R. Chitra, and P. W. Phillips, Physical Review B **103**, 125146 (2021).

[31] M. He, Y. Li, J. Cai, Y. Liu, K. Watanabe, T. Taniguchi, X. Xu, and M. Yankowitz, Nature Physics **17**, 26 (2021).

[32] Y. Jiang, J. Mao, J. Duan, X. Lai, K. Watanabe, T. Taniguchi, and E. Y. Andrei, Nano letters **17**, 2839 (2017).

[33] S. P. Milovanović, M. Anđelković, L. Covaci, and F. M. Peeters, Phys. Rev. B **102**, 245427 (2020).

[34] J. Mao, S. P. Milovanović, M. Anđelković, X. Lai, Y. Cao, K. Watanabe, T. Taniguchi, L. Covaci, F. M. Peeters, A. K. Geim, *et al.*, Nature **584**, 215 (2020).

[35] A. L. Manesco, J. L. Lado, E. V. Ribeiro, G. Weber, and D. Rodrigues Jr, 2D Materials **8**, 015011 (2020).

[36] A. L. Manesco and J. L. Lado, 2D Materials **8**, 035057 (2021).

[37] D. Giambastiani, F. Colangelo, A. Tredicucci, S. Roddaro, and A. Pitanti, Journal of Applied Physics **131**, 085103 (2022).

[38] S. A. A. Ghorashi, A. Dunbrack, J. Sun, X. Du, and J. Cano, arXiv preprint arXiv:2206.13501 (2022).

[39] J. Dong, J. Wang, and L. Fu, arXiv preprint arXiv:2208.10516 (2022).

[40] V. T. Phong and E. J. Mele, Phys. Rev. Lett. **128**, 176406 (2022).

[41] Q. Gao, J. Dong, P. Ledwith, D. Parker, and E. Khalaf, arXiv preprint arXiv:2211.00658 (2022).

[42] C. De Beule, V. T. Phong, and E. Mele, arXiv preprint arXiv:2209.02554 (2022).

[43] X. Wan, S. Sarkar, K. Sun, and S.-Z. Lin, (2023), 10.48550/arXiv.2302.07199, arXiv:2302.07199 [cond-mat].

[44] M. Katsnelson, *Graphene: Carbon in Two Dimensions* (Cambridge University Press, 2012).

[45] Y.-H. Wu, J. K. Jain, and K. Sun, Phys. Rev. B **86**, 165129 (2012).

[46] R. Roy, Physical Review B **90**, 165139 (2014).

[47] P. J. Ledwith, G. Tarnopolsky, E. Khalaf, and A. Vishwanath, Physical Review Research **2**, 023237 (2020).

[48] P. J. Ledwith, E. Khalaf, and A. Vishwanath, Annals of Physics **435**, 168646 (2021).

[49] J. Wang, J. Cano, A. J. Millis, Z. Liu, and B. Yang, Physical Review Letters **127**, 246403 (2021).

[50] B. Mera and T. Ozawa, Physical Review B **104**, 115160 (2021).

[51] P. J. Ledwith, A. Vishwanath, and E. Khalaf, Physical Review Letters **128**, 176404 (2022).

[52] M. Angeli and A. H. MacDonald, Proceedings of the National Academy of Sciences **118**, e2021826118 (2021).

[53] K. Sun, H. Yao, E. Fradkin, and S. A. Kivelson, Physical review letters **103**, 046811 (2009).

[54] J. Nilsson, A. CastroNeto, F. Guinea, and N. Peres, Physical Review B **78**, 045405 (2008).

[55] A. C. Neto, F. Guinea, N. M. Peres, K. S. Novoselov, and A. K. Geim, Reviews of modern physics **81**, 109 (2009).

[56] "See Supplemental Material ... for details, including the following: the construction of wave-function corresponding to exact flat bands, a description of symmetries required for exact flat band, example of exact flat band in $p31m$ space group, proof of fragile topology of the flat bands, construction of exact ground states of interacting Hamiltonian, and effect of chiral symmetry breaking, which includes refs. [69–75],".

[57] I. Mazin, H. O. Jeschke, F. Lechermann, H. Lee, M. Fink, R. Thomale, and R. Valentí, Nature communications **5**, 4261 (2014).

[58] D. Mumford, *Tata Lectures on Theta I* (Birkhäuser Boston, MA, 1983).

[59] Z.-D. Song, B. Lian, N. Regnault, and B. A. Bernevig, Phys. Rev. B **103**, 205412 (2021).

[60] N. Bultinck, E. Khalaf, S. Liu, S. Chatterjee, A. Vishwanath, and M. P. Zaletel, Physical Review X **10**, 031034 (2020).

[61] B. Lian, Z.-D. Song, N. Regnault, D. K. Efetov, A. Yazdani, and B. A. Bernevig, Physical Review B **103**, 205414 (2021).

[62] J. S. Hofmann, E. Khalaf, A. Vishwanath, E. Berg, and J. Y. Lee, Physical Review X **12**, 011061 (2022).

[63] K. Sun, W. V. Liu, A. Hemmerich, and S. Das Sarma, Nature Physics **8**, 67 (2012).

[64] M. Malki and G. Uhrig, Physical Review B **99**, 174412 (2019).

[65] C. Li and L. Ma, Physica B: Condensed Matter **590**, 412228 (2020).

[66] T. Yang, C. Xie, H. Chen, X. Wang, and G. Zhang, Physical Review B **105**, 094310 (2022).

[67] W.-W. Yu, Y. Liu, L. Tian, T. He, X. Zhang, and G. Liu, Journal of Physics: Condensed Matter **34**, 155703 (2022).

[68] P. M. Eugenio and O. Vafek, arXiv preprint arXiv:2208.11142 (2022).

[69] M. I. Aroyo, J. M. Perez-Mato, C. Capillas, E. Kroumova, S. Ivantchev, G. Madariaga, A. Kirov, and H. Wondratschek, Zeitschrift für Kristallographie-Crystalline Materials **221**, 15 (2006).

[70] M. I. Aroyo, A. Kirov, C. Capillas, J. Perez-Mato, and H. Wondratschek, Acta Crystallographica Section A: Foundations of Crystallography **62**, 115 (2006).

[71] M. I. Aroyo, J. M. Perez-Mato, D. Orobengoa, E. Tasci, G. de la Flor, and A. Kirov, Bulg. Chem. Commun **43**, 183 (2011).

[72] Z.-D. Song, L. Elcoro, and B. A. Bernevig, Science **367**, 794 (2020).

[73] B. A. Bernevig, Z.-D. Song, N. Regnault, and B. Lian, Physical Review B **103**, 205413 (2021).

[74] B. A. Bernevig, Z.-D. Song, N. Regnault, and B. Lian, Phys. Rev. B **103**, 205411 (2021).

[75] H. Suzuura and T. Ando, Physical review B **65**, 235412 (2002).